colorants

MDPI

Article

Comparison of the In Vitro Photodynamic Activity of the C1α and C1β Anomers of a Glucosylated Boron Dipyrromethene

Junlong Xiong [1], Ka-Wing Yeung [2], Clarence T. T. Wong [1,3], Wing-Ping Fong [2,*] and Dennis K. P. Ng [1,*]

[1] Department of Chemistry, The Chinese University of Hong Kong, Shatin, N.T., Hong Kong, China; junlong0727@163.com (J.X.); clarence-tt.wong@polyu.edu.hk (C.T.T.W.)
[2] School of Life Sciences, The Chinese University of Hong Kong, Shatin, N.T., Hong Kong, China; yeungkawing223@yahoo.com.hk
[3] Department of Applied Biology and Chemical Technology, The Hong Kong Polytechnic University, Kowloon, Hong Kong, China
* Correspondence: wpfong@cuhk.edu.hk (W.-P.F.); dkpn@cuhk.edu.hk (D.K.P.N.)

Abstract: Photodynamic therapy (PDT) is an established treatment modality for a range of superficial and localized cancers. There has been tremendous interest in the development of advanced photosensitizers that exhibit superior photophysical properties, high tumor selectivity, and improved pharmacokinetics. Glucose is one of the well-studied targeting moieties that can deliver various therapeutic agents to cancer cells selectively via the Warburg effect. However, the use of glucosylated photosensitizers for targeted PDT has remained little studied and to the best of our knowledge, the PDT effect of the positional isomers of these conjugates has never been compared. We report herein the preparation and photophysical properties of the C1α and C1β anomers of a glucosylated boron dipyrromethene-based photosensitizer. The cellular uptake and photocytotoxicity of both anomers were also studied and compared using A549 human lung carcinoma cells and HEK293 human embryonic kidney cells. Interestingly, the cellular uptake of the C1α anomer was approximately 2-fold higher than that of the C1β anomer regardless of the cell type and incubation time. The uptake pathway of both anomers was also studied. It was found that they were internalized through energy-dependent receptor/protein-mediated endocytosis rather than the well-known glucose transporters and sodium-driven glucose symporters.

Keywords: anomers; BODIPY; glucose; photodynamic therapy; photosensitizers

Citation: Xiong, J.; Yeung, K.-W.; Wong, C.T.T.; Fong, W.-P.; Ng, D.K.P. Comparison of the In Vitro Photodynamic Activity of the C1α and C1β Anomers of a Glucosylated Boron Dipyrromethene. *Colorants* **2022**, *1*, 193–207. https://doi.org/10.3390/colorants1020012

Academic Editor: Anthony Harriman

Received: 15 March 2022
Accepted: 27 April 2022
Published: 2 May 2022

1. Introduction

D-Glucose is the primary energy source of living organisms. Its cellular uptake is mediated by the membrane-bound glucose transporters, including the major glucose facilitators GLUTs, the sodium-driven glucose symporters SGLTs, and the recently identified SWEETs [1]. Among the 14 human GLUTs reported so far, only GLUT1-GLUT4 have been extensively studied and only GLUT1 and GLUT3 have been structurally characterized. It has been reported that these glucose transporters, particularly GLUT1, are overexpressed in various cancer cells in response to the higher rate of glycolysis, and the expression levels in biopsy samples correlate well with the prognosis [2,3]. On the basis of this Warburg effect [4], a large number of glucoconjugated theranostic agents have been studied with a view to achieving specific delivery to cancer cells for cancer imaging and therapy [5,6]. A well-known example is the radiolabeled glucose derivative ^{18}F-FDG, which is widely used for positron emission tomography imaging [7].

Glycoconjugation of various anticancer drugs, such as paclitaxel, glufosfamide, chlorambucil, and triptotide, has been reported [8–10]. The introduction of sugar moieties generally enhances their water solubility and stability, and when a GLUT substrate is used, it can also enable specific targeting to cancer cells. Apart from the organic anticancer drugs, the well-known platinum-based counterparts have also been glycosylated [11,12].

In particular, Lippard et al. synthesized all the possible positional isomers (C1α, C1β, C2, C3, C4, and C6) of a glucose-platinum conjugate and evaluated their in vitro and in vivo biological activities [12]. It was found that the site of substitution affected not only the cellular uptake and cytotoxicity, but also the specificity toward GLUT1. Through a series of control experiments, they also revealed that the C2-substituted conjugate exhibited the highest GLUT1-specific internalization. In tumor-bearing nude mice, the tumor uptake of this conjugate was also significantly higher than that of the non-glucosylated analogue. This represents the first study of the biological activities of a complete set of positional isomers of a given glycoconjugate.

Over the last few decades, photodynamic therapy (PDT) has emerged as a promising treatment modality for a range of cancers [13]. To enhance the therapeutic efficacy, various approaches have been explored to improve the tumor specificity of the photosensitizers, such as conjugation with tumor-targeting ligands [14], encapsulation in multifunctional nanocarriers [15], and incorporation of control units for selective activation [16]. As a major class of biomolecules, sugars have been widely used as potential tumor-targeting ligands. Glycoconjugation of various classes of photosensitizers, including porphyrins, phthalocyanines, chlorins, bacteriochlorins, corroles, porphyrazines, and boron dipyrromethenes (BODIPYs) have been prepared and evaluated for their photodynamic activities [17,18]. Generally, glycoconjugation can enhance the solubility of these macrocyclic compounds in aqueous media and promote cellular uptake, resulting in higher photocytotoxicity. However, the uptake pathways have not been unambiguously elucidated in most cases. The effect of the substitution position on the cellular uptake and photodynamic activity has also been little studied. As a result, we initiated this study and report herein the synthesis, photophysical properties, cellular uptake, and photocytotoxicity of two anomers of a glucose-conjugated BODIPY. Although a large number of BODIPY-based photosensitizers have been reported [19,20], the glycoconjugated analogues remain relatively rare [21–28].

2. Experimental

2.1. Materials and Methods

N,*N*-Dimethylformamide (DMF), tetrahydrofuran (THF), CH_2Cl_2, and toluene were purified using an Inert Solvent Purification System prior to use. All other solvents were of analytical grade and used as received without further purification. All the reactions were performed under an atmosphere of nitrogen and monitored by thin layer chromatography (TLC; Merck pre-coated silica gel 60 F254 plates). Chromatographic purification was performed on a silica gel (Macherey-Nagel, 230–400 mesh) column with the indicated eluent. Size-exclusion chromatography was performed on Bio-Beads S-X1 beads (200–400 mesh) with THF as the eluent. ^{1}H and ^{13}C{^{1}H} NMR spectra were recorded on a Bruker Avance III 400 spectrometer (^{1}H, 400 MHz; ^{13}C, 100.6 MHz) or a Bruker Avance III 500 spectrometer (^{1}H, 500 MHz; ^{13}C, 125.7 MHz) in deuterated solvents. Spectra were referenced internally by using the residual solvent {^{1}H, δ = 7.26 (for $CDCl_3$), δ = 3.31 (for CD_3OD), δ = 2.50 [for dimethylsulfoxide (DMSO)-d_6]} or solvent [^{13}C, δ = 77.2 (for $CDCl_3$), δ = 49.0 (for CD_3OD), δ = 39.5 (for DMSO-d_6)] resonances relative to $SiMe_4$. High-resolution electrospray ionization (ESI) mass spectra were recorded on a Thermo Finnigan MAT 95 XL mass spectrometer or a Bruker SolariX 9.4 Tesla FTICR mass spectrometer. UV-Vis and steady-state fluorescence spectra were taken on a Shimazu UV-1800 UV-Vis spectrophotometer and a Horiba FluoroMax-4 spectrofluorometer, respectively. BODIPY **7** was prepared as described [29].

2.2. Chemical Synthesis

2.2.1. Preparation of **3**

Sodium (1.21 g, 52.6 mmol) was added to a solution of 2-methoxyethanol (**1**) (20.0 g, 0.26 mol) in THF (100 mL) at 0 °C. The mixture was refluxed for 6 h, and then epichlorohydrin (**2**) (4.87 g, 52.6 mmol) was added dropwise. The resulting mixture was stirred at 50 °C overnight. After cooling, the mixture was extracted with ethyl acetate (300 mL × 3). The

combined organic phase was dried over anhydrous Na_2SO_4, filtered, and evaporated under reduced pressure. The crude product was purified by silica gel column chromatography using hexane/ethyl acetate (1:2, *v*/*v*) as the eluent to afford **3** as a colorless oil (3.94 g, 36%). ^{1}H NMR (400 MHz, $CDCl_3$): δ 3.97–4.02 (m, 1 H, CH), 3.63–3.66 (m, 4 H, OCH_2), 3.48–3.59 (m, 8 H, OCH_2), 3.37 (s, 6 H, CH_3). $^{13}C\{^1H\}$ (100.6 MHz, $CDCl_3$): δ 72.7, 72.0, 70.9, 69.6, 59.1. HRMS (ESI): *m*/*z* calculated for $C_9H_{20}NaO_5$ $[M + Na]^+$ 231.1202, found 231.1203.

2.2.2. Preparation of **4**

A mixture of **3** (2.52 g, 12.1 mmol), triethylamine (5 mL, 35.8 mmol), and *p*-toluenesulfonyl chloride (2.77 g, 14.5 mmol) in CH_2Cl_2 (60 mL) was stirred at room temperature for 4 h. The mixture was then washed with brine (20 mL). The organic phase was dried over anhydrous Na_2SO_4, filtered, and evaporated under reduced pressure. The crude product was purified by silica gel column chromatography using hexane/ethyl acetate (3:2, *v*/*v*) as the eluent to give **4** as a colorless oil (4.03 g, 92%). ^{1}H NMR (400 MHz, $CDCl_3$): δ 7.80 (d, *J* = 8.4 Hz, 2 H, ArH), 7.30 (d, *J* = 8.4 Hz, 2 H, ArH), 4.66–4.71 (m, 1 H, CH), 3.61–3.68 (m, 4 H, OCH_2), 3.48–3.57 (m, 4 H, OCH_2), 3.37–3.45 (m, 4 H, OCH_2), 3.30 (s, 6 H, OCH_3), 2.43 (s, 3 H, $ArCH_3$). $^{13}C\{^1H\}$ NMR (100.6 MHz, $CDCl_3$): δ 144.6, 134.1, 129.7, 128.2, 79.7, 71.8, 70.9, 69.8, 59.1, 21.7. HRMS (ESI): *m*/*z* calculated for $C_{16}H_{26}NaO_7S$ $[M + Na]^+$ 385.1291, found 385.1290.

2.2.3. Preparation of **6**

A mixture of **4** (3.15 g, 8.7 mmol), 4-hydroxybenzaldehyde (**5**) (1.27 g, 10.4 mmol), and K_2CO_3 (3.60 g, 26.0 mmol) in DMF (80 mL) was stirred at 90 °C for 16 h. After cooling, the mixture was extracted with ethyl acetate (200 mL × 2). The combined organic phase was dried over anhydrous Na_2SO_4, filtered, and evaporated under reduced pressure. The crude product was purified by silica gel column chromatography using hexane/ethyl acetate (1:2, *v*/*v*) as the eluent to afford **6** as a colorless oil (2.04 g, 75%). ^{1}H NMR (400 MHz, $CDCl_3$): δ 9.85 (s, 1 H, CHO), 7.78 (d, *J* = 8.8 Hz, 2 H, ArH), 7.07 (d, *J* = 8.8 Hz, 2 H, ArH), 4.68–4.73 (m, 1 H, CH), 3.69–3.78 (m, 4 H, OCH_2), 3.58–3.67 (m, 4 H, OCH_2), 3.49 (t, *J* = 4.8 Hz, 4 H, OCH_2), 3.33 (s, 6 H, OCH_3). $^{13}C\{^1H\}$ NMR (100.6 MHz, $CDCl_3$): δ 190.9, 163.5, 132.0, 130.2, 116.2, 76.8, 71.9, 71.1, 70.5, 59.1. HRMS (ESI): *m*/*z* calculated for $C_{16}H_{24}NaO_6$ $[M + Na]^+$ 336.1235, found 336.1233.

2.2.4. Preparation of **9**

A mixture of BODIPY **7** (0.48 g, 1.41 mmol), propargyl bromide (**8**) (0.51 g, 4.29 mmol), and K_2CO_3 (0.58 g, 4.20 mmol) in acetone (20 mL) was stirred at room temperature overnight. The solvent was removed in vacuo, and then the residue was dissolved in CH_2Cl_2 (60 mL). The solution was washed with brine (20 mL), and the organic extract was dried over anhydrous Na_2SO_4 followed by evaporation under reduced pressure. The residue was purified by silica gel column chromatography using hexane/ethyl acetate (5:1, *v*/*v*) as the eluent to give **9** as an orange-red solid (0.48 g, 90%). ^{1}H NMR (400 MHz, $CDCl_3$): δ 7.20 (d, *J* = 8.8 Hz, 2H, ArH), 7.09 (d, *J* = 8.8 Hz, 2 H, ArH), 5.98 (s, 2 H, CH), 4.76 (d, *J* = 2.4 Hz, 2 H, OCH_2), 2.55 (s, 7 H, ≡CH and CH_3), 1.42 (s, 6 H, CH_3). $^{13}C\{^1H\}$ NMR (100.6 MHz, $CDCl_3$): δ 158.2, 155.5, 143.3, 141.6, 131.9, 129.4, 128.1, 121.3, 115.8, 78.2, 76.0, 56.2, 14.7, 14.6. HRMS (ESI): *m*/*z* calculated for $C_{22}H_{21}BF_2N_2NaO$ $[M + Na]^+$ 401.1611, found 401.1611.

2.2.5. Preparation of **10**

A solution of iodic acid (0.56 g, 3.18 mmol) in water (2 mL) was added dropwise into a mixture of **9** (0.48 g, 1.27 mmol) and iodine (0.81 g, 3.18 mmol) in ethanol (40 mL). The mixture was heated at 50 °C for 3 h. The solvent was then removed in vacuo and the residue was dissolved in CH_2Cl_2 (100 mL). The solution was washed with saturated aqueous Na_2SO_3 (20 mL) and brine (20 mL), and the organic extract was dried over anhydrous Na_2SO_4 followed by evaporation in vacuo. The residue was purified by silica gel column chromatography with hexane/ethyl acetate (3:1, *v*/*v*) as the eluent to give **10**

as a bright-red solid (0.69 g, 86%). ^{1}H NMR (400 MHz, $CDCl_3$) δ 7.16 (d, *J* = 8.8 Hz, 2 H, ArH), 7.11 (d, *J* = 8.8 Hz, 2 H, ArH), 4.78 (d, *J* = 2.0 Hz, 2 H, OCH_2), 2.64 (s, 6 H, CH_3), 2.57 (t, *J* = 2.0 Hz, 1 H, ≡CH), 1.43 (s, 6 H, CH_3). $^{13}C\{^{1}H\}$ NMR (100.6 MHz, $CDCl_3$): δ 158.6, 156.8, 145.5, 141.3, 131.8, 129.3, 127.8, 116.1, 85.8, 78.0, 76.2, 56.2, 17.3, 16.2. HRMS (ESI): *m*/*z* calculated for $C_{22}H_{19}BF_2I_2N_2NaO$ $[M + Na]^+$ 652.9544, found 652.9545.

2.2.6. Preparation of **11**

A mixture of **10** (0.54 g, 0.86 mmol) and **6** (2.13 g, 6.82 mmol) was dissolved in toluene (100 mL), to which glacial acetic acid (1.0 mL, 17.5 mol), piperidine (1.0 mL, 10.1 mmol), and a small amount of $Mg(ClO_4)_2$ were added. After the consumption of **10** as indicated by TLC, the mixture was evaporated under reduced pressure. The residue was purified by silica gel column chromatography using $CHCl_3$/MeOH (30:1, *v*/*v*) as the eluent. The green fraction was collected and evaporated in vacuo. The crude product was further purified by size-exclusion chromatography using THF as the eluent followed by silica gel column chromatography again using $CHCl_3$/MeOH (30:1, *v*/*v*) as the eluent to afford **11** as a dark green solid (0.33 g, 32%). ^{1}H NMR (400 MHz, $CDCl_3$) δ 8.12 (d, *J* = 16.8 Hz, 2 H, =CH), 7.55–7.60 (m, 6 H, ArH and =CH), 7.20 (d, *J* = 8.8 Hz, 2 H, ArH), 7.13 (d, *J* = 8.8 Hz, 2 H, ArH), 7.03 (d, *J* = 8.8 Hz, 4 H, ArH), 4.80 (d, *J* = 2.4 Hz, 2 H, OCH_2), 4.66 (quintet, *J* = 4.8 Hz, 2 H, OCH), 3.73–3.82 (m, 8 H, OCH_2), 3.64–3.71 (m, 8 H, OCH_2), 3.53–3.55 (m, 8 H, OCH_2), 3.38 (s, 12 H, OCH_3), 2.58 (t, *J* = 2.4 Hz, 1 H, ≡CH), 1.50 (s, 6 H, CH_3). $^{13}C\{^{1}H\}$ NMR (100.6 MHz, $CDCl_3$): δ 159.4, 158.6, 150.6, 145.8, 139.2, 133.3, 130.1, 129.8, 129.4, 128.4, 117.0, 116.6, 116.1, 82.9, 78.0, 77.4, 77.0, 76.2, 72.1, 71.2, 70.5, 59.2, 56.2, 17.8. HRMS (ESI): *m*/*z* calculated for $C_{54}H_{63}BF_2I_2N_2NaO_{11}$ $[M + Na]^+$ 1241.2483, found 1241.2501.

2.2.7. Preparation of **14β**

A mixture of 1,2,3,4,6-penta-*O*-acetyl-β-D-glucopyranose (**12**) (3.94 g, 10.0 mmol), 3-azido-1-propanol (**13**) (2.02 g, 20.0 mmol), and $BF_3.Et_2O$ (3.78 mL, 30.0 mmol) in CH_2Cl_2 (50 mL) was stirred at room temperature for 20 h. The mixture was extracted with ethyl acetate (150 mL). The organic phase was washed with saturated aqueous $NaHCO_3$ (20 mL) and brine (20 mL), and then dried over anhydrous Na_2SO_4 followed by evaporation under reduced pressure. The crude product was purified by silica gel column chromatography using hexane/ethyl acetate (4:1, *v*/*v*) as the eluent to afford **14β** as a white solid (2.37 g, 55%). ^{1}H NMR (400 MHz, $CDCl_3$) δ 5.19 (t, *J* = 9.6 Hz, 1 H, H-3), 5.07 (t, *J* = 9.6 Hz, 1 H, H-4), 4.97 (dd, *J* = 8.0, 9.6 Hz, 1 H, H-2), 4.49 (d, *J* = 8.0 Hz, 1 H, H-1), 4.25 (dd, *J* = 4.8, 12.4 Hz, 1 H, H-6a), 4.13 (dd, *J* = 2.0, 12.4 Hz, 1 H, H-6b), 3.91–3.96 (m, 1 H, H-5), 3.67–3.71 (m, 1 H, CH), 3.56–3.62 (m, 1 H, CH), 3.33–3.37 (m, 2 H, CH_2), 2.07 (s, 3 H, OAc), 2.04 (s, 3 H, OAc), 2.01 (s, 3 H, OAc), 1.99 (s, 3 H, OAc), 1.79–1.87 (m, 2 H, CH_2). $^{13}C\{^{1}H\}$ NMR (100.6 MHz, $CDCl_3$): δ 170.8, 170.4, 169.6, 169.5, 100.9, 72.9, 71.9, 71.4, 68.5, 66.6, 62.0, 48.0, 29.1, 20.9, 20.8, 20.7. HRMS (ESI): *m*/*z* calculated for $C_{17}H_{25}N_3NaO_{10}$ $[M + Na]^+$ 454.1432, found 454.1433.

2.2.8. Preparation of **14α**

A mixture of **14β** (1.63 g, 3.78 mmol) and anhydrous $FeCl_3$ (3.04 g, 18.74 mmol) in CH_2Cl_2 (60 mL) was stirred at room temperature for 48 h. The reaction was quenched by slow addition of water (20 mL). The resulting mixture was then extracted with CH_2Cl_2 (80 mL × 2). The combined organic layer was washed with brine (40 mL), and the organic extract was dried over anhydrous Na_2SO_4 and evaporated under reduced pressure. The crude product was purified by silica gel column chromatography using hexane/ethyl acetate (4:1, *v*/*v*) as the eluent to afford **14α** as a white solid (0.65 g, 40%). ^{1}H NMR (400 MHz, $CDCl_3$) δ 5.37 (t, *J* = 9.6 Hz, 1 H, H-3), 4.98 (d, *J* = 4.0 Hz, 1 H, H-1), 4.94–4.97 (m, 1 H, H-4), 4.79 (dd, *J* = 4.0, 9.6 Hz, 1 H, H-2), 4.17 (dd, *J* = 4.8, 12.4 Hz, 1 H, H-6a), 4.01 (dd, *J* = 2.4, 12.4 Hz, 1 H, H-6b), 3.89–3.93 (m, 1 H, H-5), 3.71–3.76 (m, 1 H, OCH), 3.32–3.45 (m, 3 H, OCH and N_3CH_2), 2.00 (s, 3 H, OAc), 1.98 (s, 3 H, OAc), 1.94 (s, 3 H, OAc), 1.92 (s, 3 H, OAc), 1.79–1.84 (m, 2 H, CH_2). $^{13}C\{^{1}H\}$ NMR (100.6 MHz, $CDCl_3$): δ 170.5, 170.0,

169.9, 169.5, 95.8, 70.6, 70.0, 68.5, 67.3, 64.9, 61.9, 47.9, 28.6, 20.6. HRMS (ESI): *m/z* calculated for $C_{17}H_{25}N_3NaO_{10}$ $[M + Na]^+$ 454.1432, found 454.1432.

2.2.9. Preparation of **15β**

A mixture of **11** (80.0 mg, 65.6 μmol), **14β** (56.6 mg, 131.2 μmol), CuI (6.3 mg, 33.1 μmol), and pentamethyldiethylenetriamine (PMDETA) (10 μL) in THF (10 mL) was stirred at room temperature for 6 h. The solvent was removed in vacuo, and the residue was purified by silica gel column chromatography using $CHCl_3$/MeOH (20:1, *v*/*v*) as the eluent to afford the product as a dark green solid (95.3 mg, 88%). ^{1}H NMR (400 MHz, $CDCl_3$) δ 8.12 (d, *J* = 16.4 Hz, 2 H, =CH), 7.74 (s, 1 H, triazole-H), 7.55–7.60 (m, 6 H, ArH and =CH), 7.20 (d, *J* = 8.8 Hz, 2 H, ArH), 7.15 (d, *J* = 8.8 Hz, 2 H, ArH), 7.03 (d, *J* = 8.8 Hz, 4 H, ArH), 5.13–5.27 (m, 3 H, OCH_2 and H-3), 5.10 (t, *J* = 9.6 Hz, 1 H, H-4), 5.04 (dd, *J* = 8.0, 9.6 Hz, 1 H, H-2), 4.66 (quintet, *J* = 4.8 Hz, 2 H, OCH), 4.52–4.56 (m, 2 H, H-1 and OCH), 4.42–4.49 (m, 1 H, OCH), 4.27 (dd, *J* = 4.8, 12.4 Hz, 1 H, H-6a), 4.09–4.18 (m, 1 H, H-6b), 3.86–3.91 (m, 1 H, H-5), 3.73–3.81 (m, 8 H, OCH_2), 3.63–3.70 (m, 9 H, OCH_2 and NCH), 3.53–3.55 (m, 9 H, OCH_2 and NCH), 3.38 (s, 12 H, OCH_3), 2.17–2.27 (m, 2 H, CH_2), 2.10 (s, 3 H, OAc), 2.08 (s, 3 H, OAc), 2.03 (s, 3 H, OAc), 2.02 (s, 3 H, OAc), 1.49 (s, 6 H, CH_3). ^{13}C{^{1}H} NMR (100.6 MHz, $CDCl_3$): δ 170.7, 170.4, 169.7, 169.6, 159.5, 159.4, 150.6, 145.8, 139.2, 138.5, 133.4, 130.1, 129.9, 129.4, 128.1, 123.7, 117.0, 116.6, 115.8, 100.9, 82.9, 72.8, 72.1, 72.0, 71.4, 71.2, 70.5, 68.5, 65.9, 62.2, 62.0, 59.2, 47.0, 30.3, 21.0, 20.9, 20.8, 17.9. HRMS (ESI): *m/z* calculated for $C_{71}H_{88}BF_2I_2N_5NaO_{21}$ $[M + Na]^+$ 1672.4026, found 1672.4043.

2.2.10. Preparation of **15α**

A mixture of **11** (72.0 mg, 59.1 μmol), **14α** (51.0 mg, 118.2 μmol), CuI (5.6 mg, 29.4 μmol), and PMDETA (8 μL) in THF (4 mL) was stirred at room temperature for 6 h. The solvent was removed in vacuo, and the residue was purified by silica gel column chromatography using $CHCl_3$/MeOH (20:1, *v*/*v*) as the eluent to give the product as a dark green solid (79.9 mg, 82%). ^{1}H NMR (400 MHz, $CDCl_3$) δ 8.12 (d, *J* = 16.4 Hz, 2 H, =CH), 7.74 (s, 1 H, triazole-H), 7.55–7.60 (m, 6 H, ArH and =CH), 7.20 (d, *J* = 8.8 Hz, 2 H, ArH), 7.14 (d, *J* = 8.8 Hz, 2 H, ArH), 7.03 (d, *J* = 8.8 Hz, 4 H, ArH), 5.50 (t, *J* = 9.6 Hz, 1 H, H-3), 5.28 (s, 2 H, OCH_2), 5.05–5.10 (m, 2 H, H-1 and H-4), 4.92 (dd, *J* = 4.0, 9.6 Hz, 1 H, H-2), 4.66 (quintet, *J* = 4.8 Hz, 2 H, OCH), 4.51–4.61 (m, 2 H, OCH_2), 4.28 (dd, *J* = 4.4, 12.4 Hz, 1 H, H-6a), 4.11 (dd, *J* = 2.4, 12.4 Hz, 1 H, H-6b), 4.01–4.10 (m, 1 H, H-5), 3.73–3.81 (m, 9 H, OCH_2 and NCH), 3.63–3.70 (m, 8 H, OCH_2), 3.54 (t, *J* = 4.8 Hz, 8 H, OCH_2), 3.40–3.43 (m, 1 H, NCH), 3.37 (s, 12 H, OCH_3), 2.25–2.30 (m, 2 H, CH_2), 2.11 (s, 3 H, OAc), 2.09 (s, 3 H, OAc), 2.04 (s, 3 H, OAc), 2.03 (s, 3 H, OAc), 1.49 (s, 6 H, CH_3). ^{13}C{^{1}H} NMR (100.6 MHz, $CDCl_3$): δ 170.8, 170.4, 170.2, 169.7, 159.4, 159.3, 150.6, 145.7, 143.8, 139.2, 138.4, 133.3, 130.1, 129.9, 129.4, 128.1, 123.1, 116.9, 116.6, 115.8, 96.1, 82.9, 72.0, 71.1, 70.9, 70.5, 70.2, 68.6, 67.6, 64.7, 62.2, 61.9, 59.2, 47.1, 30.1, 20.9, 20.8, 17.8. HRMS (ESI): *m/z* calculated for $C_{71}H_{88}BF_2I_2N_5NaO_{21}$ $[M + Na]^+$ 1672.4026, found 1672.4049.

2.2.11. Preparation of **16β**

A mixture of **15β** (72.1 mg, 43.7 μmol) and K_2CO_3 (30.2 mg, 0.22 mmol) in $CHCl_3$/MeOH (1:1, *v*/*v*, 8 mL) was stirred at room temperature for 6 h. The solvent was removed in vacuo, and then the residue was purified by silica gel column chromatography using $CHCl_3$/MeOH (10:1, *v*/*v*) as the eluent to give the product as a dark green solid (48.5 mg, 75%). ^{1}H NMR (500 MHz, $CDCl_3$) δ 8.11 (d, *J* = 16.5 Hz, 2 H, =CH), 7.80 (s, 1 H, triazole-H), 7.55–7.58 (m, 6 H, ArH and =CH), 7.17 (d, *J* = 8.0 Hz, 2 H, ArH), 7.13 (d, *J* = 8.0 Hz, 2 H, ArH), 7.02 (d, *J* = 9.0 Hz, 4 H, ArH), 5.23 (br s, 2 H, Glu-H), 4.64 (quintet, *J* = 5.0 Hz, 2 H, OCH), 4.58 (br s, 2 H, OCH_2), 4.33 (br s, 2 H, Glu-H), 3.88 (br s, 3 H, Glu-H), 3.73–3.80 (m, 8 H, OCH_2), 3.63–3.70 (m, 9 H, OCH_2 and NCH), 3.53 (t, *J* = 4.5 Hz, 8 H, OCH_2), 3.45 (br s, 1 H, NCH), 3.37 (s, 12 H, OCH_3), 2.20 (br s, 2 H, CH_2), 1.47 (s, 6 H, CH_3). ^{13}C{^{1}H} NMR (125.7 MHz, $CDCl_3$): δ 159.5, 159.3, 150.6, 145.8, 139.3, 138.4, 133.3, 130.1, 129.9, 129.4, 128.1, 117.0, 116.6, 115.8, 103.0, 82.9, 75.9,

73.7, 72.1, 71.1, 70.5, 70.1, 66.0, 62.0, 59.2, 47.4, 30.5, 29.9, 17.9. HRMS (ESI): *m/z* calculated for $C_{63}H_{80}BF_2I_2N_5NaO_{17}$ $[M + Na]^+$ 1504.3602, found 1504.3629.

2.2.12. Preparation of **16α**

A mixture of **15α** (62.0 mg, 37.6 μmol) and K_2CO_3 (25.9 mg, 0.19 mmol) in $CHCl_3$/MeOH (1:1, *v*/*v*, 8 mL) was stirred at room temperature for 6 h. The solvent was removed in vacuo, and then the residue was purified by silica gel column chromatography using $CHCl_3$/MeOH (10:1, *v*/*v*) as the eluent to give the product as a dark green solid (43.4 mg, 78%). ^{1}H NMR (500 MHz, $CDCl_3$): δ 8.11 (d, *J* = 16.5 Hz, 2 H, =CH), 7.79 (s, 1 H, triazole-H), 7.55–7.59 (m, 6 H, ArH and =CH), 7.18 (d, *J* = 8.0 Hz, 2 H, ArH), 7.13 (d, *J* = 8.0 Hz, 2 H, ArH), 7.02 (d, *J* = 9.0 Hz, 4 H, ArH), 5.24 (br s, 2 H, Glu-H), 4.85 (br s, 2 H, Glu-H), 4.65 (quintet, *J* = 5.0 Hz, 2 H, OCH), 4.58 (br s, 2 H, OCH_2), 3.84 (br s, 3 H, Glu-H), 3.73–3.80 (m, 9 H, OCH_2 and NCH), 3.63–3.70 (m, 8 H, OCH_2), 3.59 (br s, 1 H, NCH), 3.53 (t, *J* = 4.5 Hz, 8 H, OCH_2), 3.37 (s, 12 H, OCH_3), 2.22 (br s, 2 H, CH_2), 1.47 (s, 6 H, CH_3). ^{13}C{^{1}H} NMR (125.7 MHz, $CDCl_3$): δ 159.5, 159.3, 150.6, 145.8, 139.3, 138.4, 133.3, 130.1, 130.0, 129.4, 128.1, 117.0, 116.6, 115.8, 99.0, 82.9, 74.5, 72.4, 72.1, 71.9, 71.2, 70.6, 70.5, 64.8, 62.1, 59.2, 47.8, 30.3, 29.9, 17.9. HRMS (ESI): *m/z* calculated for $C_{63}H_{80}BF_2I_2N_5NaO_{17}$ $[M + Na]^+$ 1504.3602, found 1504.3619.

2.3. Photophysical Measurements

The fluorescence quantum yields (Φ_F) were determined by the equation [30]:

$$\Phi F_{(sample)} = \left(\frac{F_{sample}}{F_{ref}}\right)\left(\frac{A_{ref}}{A_{sample}}\right)\left(\frac{n^2_{sample}}{n^2_{ref}}\right)F_{(ref)}$$

where F, A, and n are the measured fluorescence (area under the emission peak), the absorbance at the excitation wavelength (610 nm), and the refractive index of the solvent, respectively. Zinc(II) phthalocyanine (ZnPc) in DMF was used as the reference [$\Phi_{F(ref)}$ = 0.28] [31]. To minimize re-absorption of radiation by the ground-state species, the emission spectra were obtained in very dilute solutions of which the absorbance at the excitation wavelength was less than 0.05.

The singlet oxygen quantum yields (Φ_Δ) were measured using 1,3-diphenylisobenzofuran (DPBF) as the singlet oxygen scavenger and ZnPc in DMF as the reference (Φ_Δ = 0.56). A mixture of DPBF (30 μM) and the photosensitizer (2 μM) in DMF was illuminated with red light coming from a 300 W halogen lamp after passing through a water tank for cooling and a color filter (Newport, cut-on at 610 nm). The decay of DPBF was monitored spectroscopically at its absorbance at 415 nm along with the irradiation time. The Φ_Δ values were obtained by the following equation [32]:

$$\Phi_{\Delta(s)} = \Phi_{\Delta(ref)}\ (W_s \times I_{abs(ref)})/(W_{ref} \times I_{abs(s)})$$

where $\Phi_{\Delta(ref)}$ stands for the Φ_Δ of ZnPc in DMF, W_s and W_{ref} refer to the DPBF photobleaching rates in the presence of the photosensitizer and ZnPc, respectively, and $I_{abs(s)}$ and $I_{abs(ref)}$ are the rates of light absorption by the photosensitizer and ZnPc, respectively.

2.4. Biological Studies

2.4.1. Cell Lines and Culture Conditions

A549 human lung carcinoma cells (ATCC, no. CCL–185) and HEK293 human embryonic kidney cells (ATCC, no. CRL–1573) were maintained in Dulbecco's Modified Eagle Medium (DMEM) (ThermoFisher Scientific, cat. no. 12100–046) supplemented with fetal bovine serum (FBS) (10%) and penicillin–streptomycin (100 unit mL^{-1} and 100 μg mL^{-1}, respectively). Cells were grown at 37 °C in a humidified 5% CO_2 atmosphere.

2.4.2. Flow Cytometric Analysis

Approximately 2×10^5 A549 and HEK293 cells in DMEM (2.0 mL) were seeded on 6-well culture plates and incubated overnight at 37 °C under 5% CO_2. After being rinsed with phosphate–buffered saline (PBS) (1.0 mL) twice, the cells were treated with **11**, **16α**, or **16β** (2 μM) at 37 °C for 1, 2, 4, and 6 h, respectively. The cells were then rinsed with PBS (1.0 mL) and harvested by 0.25% trypsin–EDTA (Invitrogen, 0.2 mL) for 5 min. The activity of trypsin was quenched with a serum-containing medium (0.5 mL), and the mixture was centrifuged at 1500 rpm for 3 min at room temperature. The pellet was washed with PBS (1.0 mL) and then subject to centrifugation under the same conditions. The cells were then suspended in PBS (1.0 mL) and the intracellular fluorescence intensities were measured using a BD FACSVerse flow cytometer (Becton Dickinson) with 10^4 cells counted in each sample. The photosensitizers were excited by an argon laser at 640 nm and the emitted fluorescence was monitored at 650–750 nm. The data collected were analyzed using the BD FACSuite. All experiments were performed in triplicate.

2.4.3. Confocal Fluorescence Microscopic Study

Approximately 2×10^5 A549 cells in DMEM (2.0 mL) were seeded on a glass-bottom confocal dish and incubated overnight at 37 °C in a humidified 5% CO_2 atmosphere. After being rinsed with PBS (1.0 mL) twice, the cells were treated with **16α** or **16β** (2 μM) in the medium (1.5 mL) at 4 °C or 37 °C for 4 h. After removing the medium, the cells were rinsed with PBS (1.0 mL) twice before being examined using a Leica TCS SP8 high-speed confocal microscope equipped with solid-state 488 and 638 nm lasers. The photosensitizers were excited at 638 nm and their fluorescence was monitored at 650–750 nm. The images were digitized and analyzed using a Leica Application Suite X software.

2.4.4. Cellular Uptake Inhibition Assay

Approximately 2×10^5 A549 cells in DMEM (2.0 mL) were seeded on 6-well culture plates and incubated overnight at 37 °C under 5% CO_2. After being rinsed with PBS (1.0 mL) twice, the cells were pre-incubated in the medium at 37 °C for 2 h with or without the addition of cytochalasin B (50 μM) or dapagliflozin (100 nM). A solution of **16α** or **16β** (2 μM) was then used for subsequent incubation at 37 °C for a further 4 h. The cells were then rinsed with PBS (1.0 mL) and harvested by 0.25% trypsin–EDTA (Invitrogen, 0.2 mL) for 5 min. The activity of trypsin was quenched with a serum-containing medium (0.5 mL), and the mixture was centrifuged at 1500 rpm for 3 min at room temperature. The pellet was washed with PBS (1.0 mL) and then subject to centrifugation under the same conditions. The cells were then suspended in PBS (1.0 mL) and the intracellular fluorescence intensities were measured using a BD FACSVerse flow cytometer (Becton Dickinson) with 10^4 cells counted in each sample. The photosensitizers were excited by an argon laser at 640 nm and the emitted fluorescence was monitored at 650–750 nm. The data collected were analyzed using the BD FACSuite. All experiments were performed in triplicate.

2.4.5. Study of Subcellular Localization

Approximately 2×10^5 A549 cells in DMEM (2.0 mL) were seeded on a glass-bottom confocal dish and incubated at 37 °C overnight in a humidified 5% CO_2 atmosphere. After being rinsed with PBS (1.0 mL) twice, the cells were treated with **16α** or **16β** (2 μM) at 37 °C for 4 h. After being washed twice with PBS (1.0 mL) twice, the cells were suspended in Hank's balanced salt solution (1.0 mL) with LysoTracker Green DND-26 (Thermo Fisher Scientific Inc., L7526, 1.5 μM) at 37 °C for 20 min. After removing the solution, the cells were rinsed with PBS (1.0 mL) twice before being examined using a Leica TCS SP8 high-speed confocal microscope equipped with solid-state 488 and 638 nm lasers. The LysoTracker was excited at 488 nm and its fluorescence was monitored at 500–570 nm, while **16α** and **16β** were excited at 638 nm and their fluorescence was monitored at 650–750 nm.

2.4.6. Photocytotoxicity Assay

Approximately 2×10^4 A549 or HEK293 cells per well in DMEM were inoculated in 96-well culture plates and incubated overnight at 37 °C in a humidified 5% CO_2 atmosphere. A stock solution of **16α** or **16β** (40 μM) was prepared by dissolving the compound (59 μg, 40 nmol) in DMSO (40 μL). The stock solution was diluted with a serum-free DMEM to various concentrations (8.0, 4.0, 2.0, 1.0, and 0.5 μM by two-fold dilution). The cells, after being rinsed with PBS twice, were treated with **16α** or **16β** (100 μL for each well) at various concentrations (8.0, 4.0, 2.0, 1.0, and 0.5 μM) for 6 h at 37 °C under a 5% CO_2 atmosphere. The cells were then rinsed with PBS (100 μL for each well) twice and re-fed with the fresh culture medium (100 μL for each well) before being illuminated at ambient temperature. The light source consisted of a 300 W halogen lamp, a water tank for cooling, and a color glass filter (Newport) cut-on at 610 nm. The fluence rate (λ > 610 nm) was 23 mW cm^{-2}. Illumination of 20 min led to a total fluence of 28 J cm^{-2}. Cell viability was determined by means of a colorimetric 3-(4,5-dimethylthiazol-2-yl)-2,5-diphenyltetrazolium bromide (MTT) assay [33]. After illumination, the cells were incubated at 37 °C under 5% CO_2 overnight. A MTT (Sigma) solution in PBS (3 mg mL^{-1}, 50 μL) was added to each well followed by incubation for 4 h under the same environment. DMSO (100 μL) was then added to each well. Solutions in all the wells were mixed until homogenous. The absorbance at 490 nm of each well on the plate was taken by a microplate reader (Tecan Spark 10M) at ambient temperature. The average absorbance of the blank wells, which did not contain the cells, was subtracted from the readings of the other wells. The cell viability was then determined by the equation:

$$\% \text{ viability} = \frac{\sum\left(\frac{A_i}{A_{control}}\right) \times 100}{n}$$

where A_i is the absorbance of the ith datum (i = 1, 2, . . . , n), $A_{control}$ is the average absorbance of the control wells in which the compound was absent, and n (=4) is the number of data points.

3. Results and Discussion

3.1. Synthesis and Characterization

Owing to the ease of chemical modification and tunable electronic absorption and photophysical properties, BODIPYs are promising photosensitizers for PDT [19,20] and were therefore selected for this study. Scheme 1 shows the synthetic route used to prepare the BODIPY-based photosensitizing component. 2-Methoxyethanol (**1**) was first treated with sodium. The alkoxide formed in situ was then treated with epichlorohydrin (**2**) to give the substituted product **3**, which was tosylated to afford **4**. It then underwent nucleophilic substitution with 4-hydroxybenzaldehyde (**5**) in the presence of K_2CO_3 in DMF to give benzaldehyde **6**. For the BODIPY part, the previously reported phenol-substituted analogue **7** [29] was used as the starting material. Treatment of this compound with propargyl bromide (**8**) and K_2CO_3 gave **9**. To promote intersystem crossing and the formation of singlet oxygen through the heavy-atom effect [34], **9** was iodinated using a mixture of iodine and iodic acid in ethanol to give the diiodo product **10**, which underwent Knoevenagel condensation with benzaldehyde **6** to afford distyryl BODIPY **11**. With two branched ethylene glycol moieties, this compound was expected to exhibit enhanced solubility and reduced aggregation tendency in aqueous media.

With an alkynyl moiety, this BODIPY could be coupled with an azide-substituted D-glucose readily through copper-promoted alkyne-azide cycloaddition reaction. As shown in Scheme 2, treatment of 1,2,3,4,6-penta-*O*-acetyl-β-D-glucopyranose (**12**) with 3-azido-1-propanol (**13**) in the presence of $BF_3{\cdot}OEt_2$ afforded **14β** with the azide-containing substituent at the C1β position. For the conversion to the α-anomer, **14β** was treated with anhydrous $FeCl_3$ to mediate the anomerization [35], giving the α-anomer **14α**. The C1 anomeric proton resonated as a doublet at δ 4.49 ppm with a coupling constant of

8.0 Hz for **14β** in the ^{1}H NMR spectrum, while that for **14α** appeared as a doublet at δ 4.98 ppm with a coupling constant of 4.0 Hz, which are the typical spectral features of C1β and C1α anomers, respectively. In addition, the ^{13}C NMR signal of the C1 carbon was also significantly different for the two anomers (δ 100.9 and 95.8 ppm for **14β** and **14α**, respectively), which also supported the assignment of the stereochemistry. Both **14β** and **14α** could "click" with **11** readily in the presence of CuI and PMDETA to give the corresponding conjugates **15β** and **15α**, respectively. Upon alkaline hydrolysis, these compounds underwent deacetylation to give the C1β and C1α anomeric glucosylated BODIPY derivatives **16β** and **16α**, respectively. Both conjugates could be purified readily using chromatography on a silica gel column and were characterized with various spectroscopic methods.

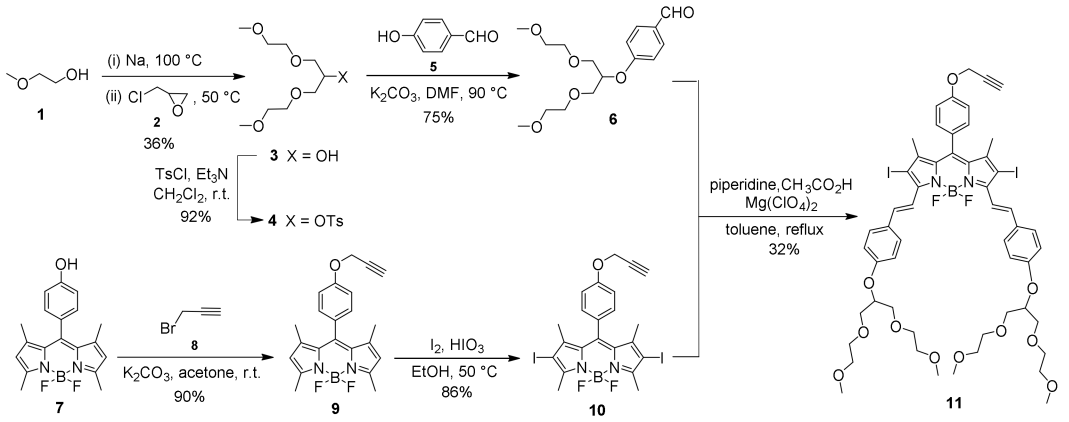

Scheme 1. Synthetic scheme of alkynyl distyryl BODIPY **11**.

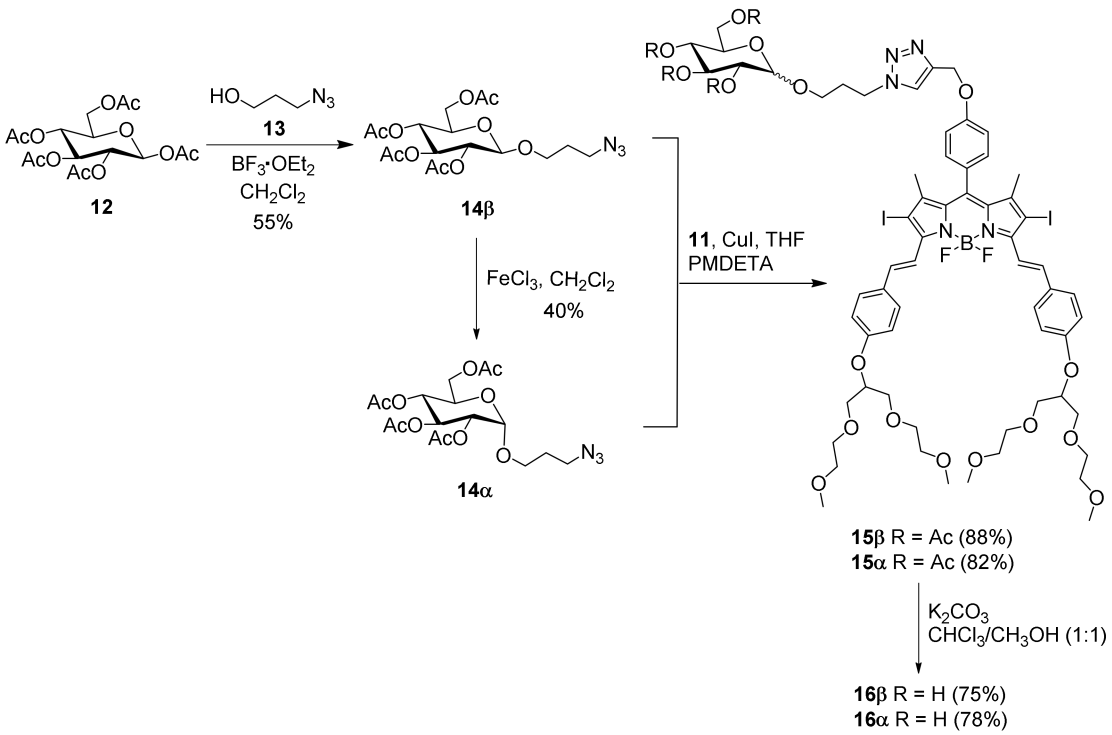

Scheme 2. Synthetic scheme of the anomeric glucosylated BODIPY derivatives **16β** and **16α**.

UV-Vis and fluorescence spectra of **16α** and **16β** were first measured in DMF (Figure S1 in the Supporting Information). The absorption spectra were essentially the same, showing

typical absorptions of distyryl BODIPYs. The longest-wavelength absorption appeared at 662 nm, which strictly followed the Beer-Lambert law, suggesting that both anomers were not aggregated in DMF (Figure S2 in the Supporting Information). Upon excitation at 610 nm, both compounds showed a fluorescence band at 689 nm with a fluorescence quantum yield (Φ_F) of 0.18 relative to ZnPc (Φ_F = 0.28). By using DPBF as the singlet oxygen probe, the singlet oxygen generation efficiency of both compounds was also evaluated. As shown in Figure S3a in the Supporting Information, both of them could effectively trigger the photodecay of DPBF as shown by the decrease in the absorbance of its absorption at 415 nm along with the irradiation time, from which the singlet oxygen quantum yield could be determined. The values (Φ_Δ = 0.42 for **16α** and 0.41 for **16β**) were just slightly lower than that of ZnPc (Φ_Δ = 0.56). These data are summarized in Table 1. The spectral and photophysical properties of these two anomers were also measured in PBS with 0.1% Tween 80 (*v*/*v*) added to increase the water solubility of the conjugates (Figures S3b and S4 in the Supporting Information). The results were very similar to those measured in DMF.

Table 1. Electronic absorption and photophysical properties of **16α** and **16β** in DMF.

Compound	λ_{max}/nm (log ε)	λ_{em} [a]/nm	Φ_F [b]	Φ_Δ [c]
16α	319 (4.24), 379 (4.52), 447 (4.14), 662 (4.82)	689	0.18	0.42
16β	320 (4.23), 379 (4.52), 448 (4.13), 662 (4.81)	689	0.18	0.41

[a] Excited at 610 nm. [b] Using ZnPc in DMF as the reference (Φ_F = 0.28). [c] Using ZnPc in DMF as the reference (Φ_Δ = 0.56).

3.2. Cellular Uptake

The in vitro properties of these two anomers were then studied using A549 human lung carcinoma cells and HEK293 human embryonic kidney cells. The former is known to exhibit the Warburg effect [4], while the latter is a normal cell type that was used as the negative control. We first examined the cellular uptake of these two compounds using flow cytometry. After incubation (at 2 μM) for 6 h, the intracellular fluorescence intensities were measured, which could reflect the extent of cellular uptake. As shown in Figure 1a, the intensity generally followed the order: **16α** > **16β** for both cell lines and A549 > HEK293 for both anomers. Interestingly, the intensities were much higher than those for the non-glucosylated analogue **11** against both the cell lines. The strongest intracellular fluorescence was observed for **16α** in A549 cells, of which the intensity was about 7-fold higher than that in HEK293 cells. In addition, we also compared the fluorescence intensities of **16α** and **16β** in A549 cells after incubation for different periods of time. As for small molecular-based photosensitizers, incubation for a few hours is usually long enough to deliver a sufficient amount of the dyes into the cells for fluorescence imaging and PDT [21,22,24,36,37], and the results shown in Figure 1a indicate that incubation with these two compounds for 6 h already led to strong intracellular fluorescence intensities, we chose the period from 1 to 6 h in this study. As shown in Figure 1b, the intensity of **16α** was consistently higher than that of **16β** by about 2-fold for all the incubation times. The results demonstrated that the glucose moiety greatly promoted the internalization of the BODIPY core, particularly against the cancer cells, and the α-anomer **16α** exhibited significantly higher cellular uptake than the β-anomer **16β**.

It is worth noting that Lippard et al. compared the cytotoxicity of all the possible positional isomers of a glucose-platinum conjugate and found that the cellular uptake of the C1α anomer was slightly higher than that of the C1β anomer for a range of cancer cell lines, and GLUT1 was the transporter responsible for the uptake [12]. However, He et al. conjugated triptolide with glucose via C1α and C1β linkages [9]. The results demonstrated that the C1β conjugate exhibited higher uptake and lower IC_{50} value than the C1α counterpart. It seems that the binding affinity of the glucose moiety is greatly affected by the conjugated drug component. In attempts to reveal the cellular internalization mechanism of **16α** and **16β**, further in vitro studies were carried out as reported below.

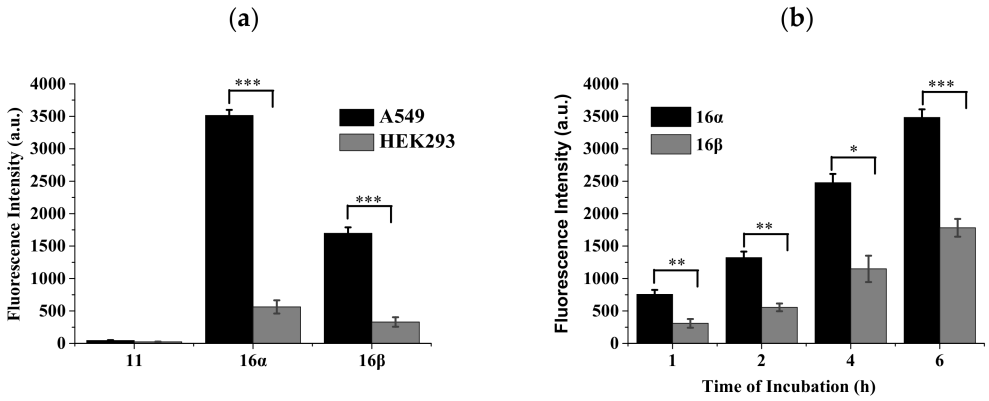

Figure 1. (**a**) Intracellular fluorescence intensities of A549 and HEK293 cells after incubation with **11**, **16α**, or **16β** (2 μM) for 6 h determined by flow cytometry. Data are reported as mean ± standard deviation (SD) of three independent experiments. *** $p < 0.01$. (**b**) Intracellular fluorescence intensities of A549 cells after incubation with **16α** or **16β** (2 μM) for 1, 2, 4, and 6 h. Data are reported as mean ± SD of three independent experiments. * $p < 0.05$, ** $p < 0.01$, *** $p < 0.001$.

First, we examined whether GLUTs were involved. These unique channels can mediate the bidirectional transport of monosaccharides across the cell membrane down their concentration gradient in an energy-independent manner [1]. Thus, we studied and compared the cellular uptake of **16α** and **16β** against A549 cells at 4 °C and 37 °C to reveal whether they are internalized via an energy-dependent or energy-independent pathway. If they are internalized via GLUTs, the cellular uptake should not be affected by the incubation temperature. Unexpectedly, the fluorescence intensity was almost invisible for both compounds at 4 °C, showing that the cellular uptake was greatly inhibited. In contrast, bright intracellular fluorescence was observed for incubation at 37 °C (Figure 2). The results suggested that the internalization of **16α** and **16β** was mediated by an energy-dependent pathway and did not involve the GLUTs. This was further supported by the study using the GLUTs inhibitor cytochalasin B [12]. As shown in Figure 3a, the fluorescence intensity as determined by flow cytometry was not significantly changed when cytochalasin B (50 μM) was added during the incubation with **16α** or **16β** (2 μM) for 4 h at 37 °C.

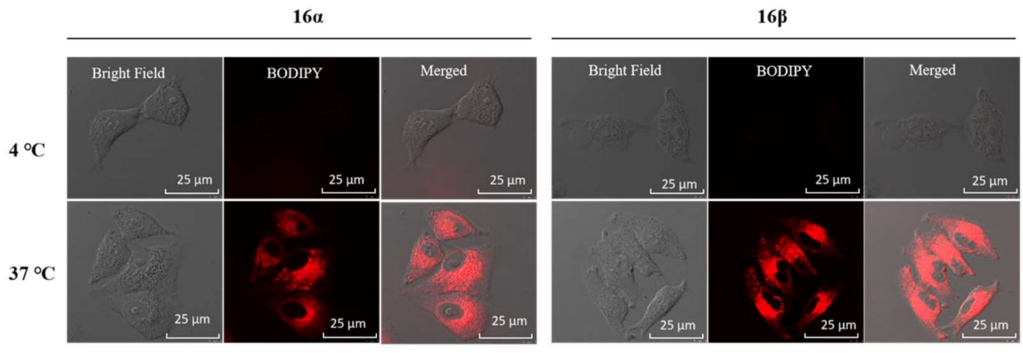

Figure 2. Bright-field, fluorescence, and the merged confocal images of A549 cells after incubation with **16α** or **16β** (2 μM) for 4 h.

Besides GLUTs, the SGLTs are also common transporters for glucose uptake, which are overexpressed in a range of cancer cells [38,39]. However, unlike the GLUTs, the SGLT-mediated uptake is an energy-dependent process which requires the use of adenosine triphosphate. To reveal whether this pathway was involved in the uptake of **16α** and **16β**, the SGLTs inhibitor dapagliflozin [40] (100 nM) was added during the drug incubation (at 2 μM) for 4 h at 37 °C, and then the intracellular fluorescence intensities were determined by flow cytometry. As shown in Figure 3b, the intensities remained unchanged upon

addition of dapagliflozin for both compounds, showing that their cellular uptake also did not involve the SGLTs.

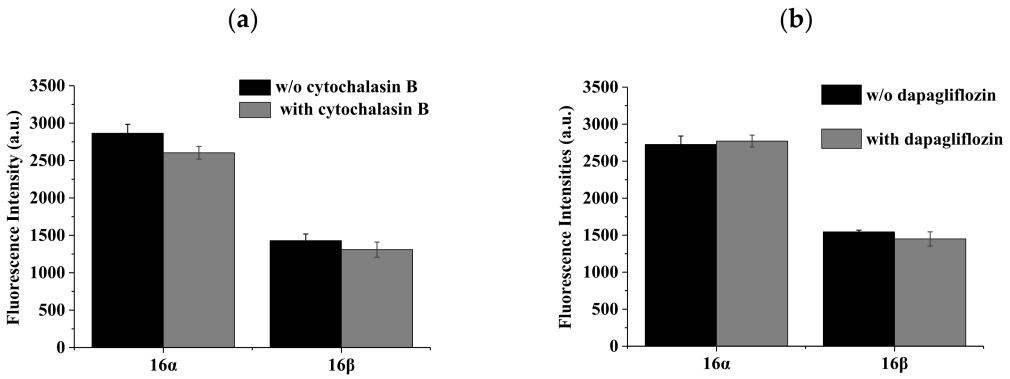

Figure 3. Intracellular fluorescence intensities of A549 cells after incubation with **16α** or **16β** (2 μM) for 4 h at 37 °C with or without the addition of (**a**) cytochalasin B (50 μM) and (**b**) dapagliflozin (100 nM) determined by flow cytometry. Data are reported as mean ± SD of three independent experiments.

Furthermore, for transporter-mediated internalization, the compounds should be distributed evenly in the cytoplasm. Hence, we further examined the subcellular localization of **16α** and **16β** in A549 cells after incubation for 4 h. As shown in Figure 4, the fluorescence due to these two compounds could overlap well with that due to LysoTracker Green and the co-localization coefficient was found to be 0.725 and 0.760 for **16α** and **16β**, respectively. These results suggested that both compounds were taken up by the cells through endocytosis, for which they are trafficked sequentially to the early endosomes, the late endosomes, and eventually the lysosomes [41]. The preferential localization of these compounds in lysosomes further precluded the uptake through the two conventional GLUTs and SGLTs. Although the actual uptake pathway of **16α** and **16β** remains elusive at this stage, it was found that they are internalized through an energy-dependent endocytosis process and the cellular uptake of **16α** is significantly higher than that of **16β**.

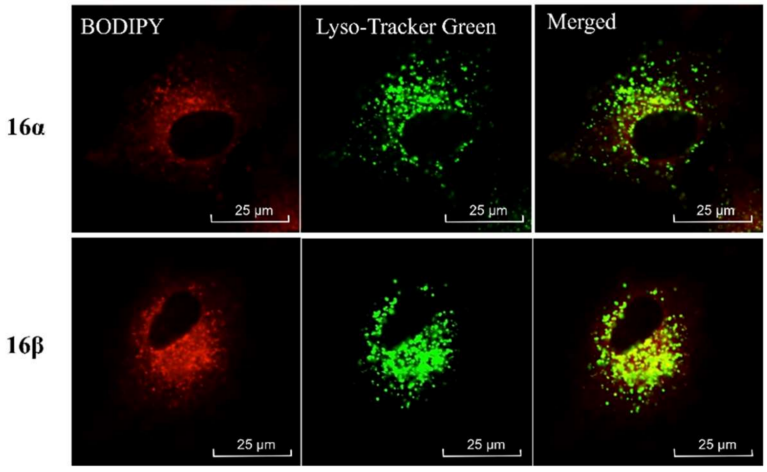

Figure 4. Confocal fluorescence images of A549 cells after incubation with **16α** or **16β** (2 μM) for 4 h, followed by staining with LysoTracker Green (1.5 μM) for 20 min.

3.3. Photocytotoxicity

The cytotoxic effect of these two anomers was then studied and compared against A549 and HEK293 cells by MTT assay, both in the absence and presence of light irradiation. The corresponding dose-dependent survival curses are shown in Figure 5. It can be observed

that both anomers were not cytotoxic in the dark toward the two cell lines. Upon irradiation ($\lambda > 610$ nm, 23 mW cm^{-2}, 28 J cm^{-2}), they became highly photocytotoxic toward A549 cells. The IC_{50} value was found to be 0.7 and 1.5 μM for **16α** and **16β**, respectively. The higher photocytotoxicity of the former could be attributed to its higher cellular uptake reported above. Interestingly, the photocytotoxicity was significantly reduced for HEK293 cells as a result of the lower uptake by these non-cancerous cells. The results demonstrated that **16α** and **16β** have a cell-selective property and the former is a particularly potent photosensitizer for PDT.

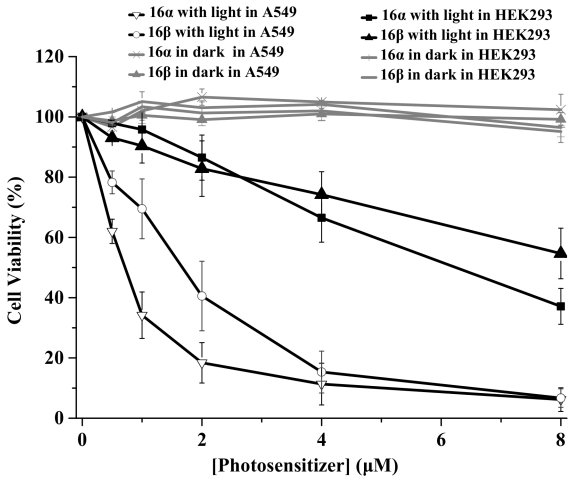

Figure 5. Comparison of the cytotoxic effect of **16α** and **16β** against A549 and HEK293 cells, both in the absence and presence of light irradiation ($\lambda > 610$ nm, 23 mW cm^{-2}, 28 J cm^{-2}). The cells were incubated with the photosensitizers for 6 h, followed by the dark or light treatment. Data are reported as mean ± standard error of the mean of three independent experiments, each performed in quadruplicate.

4. Conclusions

In summary, we have synthesized and characterized two anomeric glucosylated distyryl BODIPY-based photosensitizers **16α** and **16β**. They showed relatively strong fluorescence emission and behaved as efficient singlet oxygen generators, both in DMF and in aqueous media. Through a series of in vitro experiments, it was found that they could be taken up selectively by A549 cancer cells, while for the non-cancerous HEK293 cells, the intracellular fluorescence intensities were ca. 6- to 7-fold weaker. As a result, both anomers exhibited higher photocytotoxicity toward the former cell line with an IC_{50} value of 0.7 and 1.5 μM for **16α** and **16β**, respectively. The higher potency of the α-anomer **16α** could be attributed to its 2-fold higher cellular uptake than the β-anomer **16β**. The uptake of these anomers was through an energy-dependent endocytosis pathway, but not via the common GLUTs and SGLTs. It is worth noting that Kamkaew et al. reported two bis(glucose)-substituted aza-BODIPYs that exhibited enhanced cellular uptake toward the GLUTs-overexpressed breast cancer cells [24]. Based on the reduced uptake in the presence of D-glucose or a glucose metabolism suppressor (combretastatin), it was suggested that GLUTs were involved in the uptake of the dyes. These results suggest that introduction of additional glucose moieties may assist the active uptake via the GLUTs, which could be a direction for further chemical modification of this class of photosensitizers. Nevertheless, the overall results of this study demonstrated that glucose moieties could promote the cellular uptake of BODIPYs and different anomeric forms could greatly affect the uptake and photocytotoxicity of the conjugates. The anomer **16α** reported herein serves as a potent photosensitizer for PDT.

Supplementary Materials: The supporting information can be downloaded at https://www.mdpi.com/article/10.3390/colorants1020012/s1.

Author Contributions: J.X., methodology, investigation, and writing—original draft; K.-W.Y., methodology and investigation; C.T.T.W., writing—original draft; W.-P.F., supervision and writing—review and editing; D.K.P.N., conceptualization, supervision, formal analysis, and writing—review and editing. All authors have read and agreed to the published version of the manuscript.

Funding: This research received no external funding.

Institutional Review Board Statement: Not applicable.

Informed Consent Statement: Not applicable.

Data Availability Statement: Data are available in a publicly accessible repository.

Acknowledgments: The work was supported by The Chinese University of Hong Kong through a Direct Grant.

Conflicts of Interest: The authors declare no conflict of interest.

References

1. Deng, D.; Yan, N. GLUT, SGLT, and SWEET: Structural and mechanistic investigations of the glucose transporters. *Protein Sci.* **2016**, *25*, 546–558. [CrossRef] [PubMed]
2. Cairns, R.A.; Harris, I.S.; Mak, T.W. Regulation of cancer cell metabolism. *Nat. Rev. Cancer* **2011**, *11*, 85–95. [CrossRef] [PubMed]
3. Pliszka, M.; Szablewski, L. Glucose transporters as a target for anticancer therapy. *Cancers* **2021**, *13*, 4184. [CrossRef] [PubMed]
4. Vander Heiden, M.G.; Cantley, L.C.; Thompson, C.B. Understanding the Warburg effect: The metabolic requirement of cell proliferation. *Science* **2009**, *324*, 1029–1033. [CrossRef]
5. Fu, J.; Yang, J.; Seeberger, P.H.; Yin, J. Glycoconjugates for glucose transporter-mediated cancer-specific targeting and treatment. *Carbohydr. Res.* **2020**, *498*, 108195. [CrossRef]
6. Bononi, G.; Iacopini, D.; Cicio, G.; Di Pietro, S.; Granchi, C.; Di Bussolo, V.; Minutolo, F. Glycoconjugated metal complexes as cancer diagnostic and therapeutic agents. *ChemMedChem* **2021**, *16*, 30–64. [CrossRef]
7. Ben-Haim, S.; Ell, P. ^{18}F-FDG PET and PET/CT in the evaluation of cancer treatment response. *J. Nucl. Med.* **2009**, *50*, 88–99. [CrossRef]
8. Calvaresia, E.C.; Hergenrother, P.J. Glucose conjugation for the specific targeting and treatment of cancer. *Chem. Sci.* **2013**, *4*, 2319–2333. [CrossRef]
9. He, Q.-L.; Minn, I.; Wang, Q.; Xu, P.; Head, S.A.; Datan, E.; Yu, B.; Pomper, M.G.; Liu, J.O. Targeted delivery and sustained antitumor activity of triptolide through glucose conjugation. *Angew. Chem. Int. Ed.* **2016**, *55*, 12035–12039. [CrossRef]
10. Datan, E.; Minn, I.; Xu, P.; He, Q.-L.; Ahn, H.-H.; Yu, B.; Pomper, M.G.; Liu, J.O. A glucose-triptolide conjugate selectively targets cancer cells under hypoxia. *iScience* **2020**, *23*, 101536. [CrossRef]
11. Patra, M.; Johnstone, T.C.; Suntharalingam, K.; Lippard, S.J. A potent glucose-platinum conjugate exploits glucose transporters and preferentially accumulates in cancer cells. *Angew. Chem. Int. Ed.* **2016**, *55*, 2550–2554. [CrossRef] [PubMed]
12. Patra, M.; Awuah, S.G.; Lippard, S. Chemical approach to positional isomers of glucose-platinum conjugates reveals specific cancer targeting through glucose-transporter-mediated uptake in vitro and in vivo. *J. Am. Chem. Soc.* **2016**, *138*, 12541–12551. [CrossRef] [PubMed]
13. Algorri, J.F.; Ochoa, M.; Roldán-Varona, P.; Rodríguez-Cobo, L.; López-Higuera, J.M. Photodynamic therapy: A compendium of latest reviews. *Cancers* **2021**, *13*, 4447. [CrossRef] [PubMed]
14. Gierlich, P.; Mata, A.I.; Donohoe, C.; Brito, R.M.M.; Senge, M.O.; Gomes-da-Silva, L.C. Ligand-targeted delivery of photosensitizers for cancer treatment. *Molecules* **2020**, *25*, 5317. [CrossRef]
15. Lucky, S.S.; Soo, K.C.; Zhang, Y. Nanoparticles in photodynamic therapy. *Chem. Rev.* **2015**, *115*, 1990–2042. [CrossRef] [PubMed]
16. Luby, B.M.; Walsh, C.D.; Zheng, G. Advanced photosensitizer activation strategies for smarter photodynamic therapy beacons. *Angew. Chem. Int. Ed.* **2019**, *58*, 2558–2569. [CrossRef]
17. Singh, S.; Aggarwal, A.; Bhupathiraju, N.V.S.D.K.; Arianna, G.; Tiwari, K.; Drain, C.M. Glycosylated porphyrins, phthalocyanines, and other porphyrinoids for diagnostics and therapeutics. *Chem. Rev.* **2015**, *115*, 10261–10306. [CrossRef]
18. Kataoka, H.; Nishie, H.; Tanaka, M.; Sasaki, M.; Nomoto, A.; Osaki, T.; Okamoto, Y.; Yano, S. Potential of photodynamic therapy based on sugar-conjugated photosensitizers. *J. Clin. Med.* **2021**, *10*, 841. [CrossRef]
19. Kue, C.S.; Ng, S.Y.; Voon, S.H.; Kamkaew, A.; Chung, L.Y.; Kiew, L.V.; Lee, H.B. Recent strategies to improve boron dipyrromethene (BODIPY) for photodynamic cancer therapy: An updated review. *Photochem. Photobiol. Sci.* **2018**, *17*, 1691–1708. [CrossRef]
20. Sun, W.; Zhao, X.; Fan, J.; Du, J.; Peng, X. Boron dipyrromethene nano-photosensitizers for anticancer phototherapies. *Small* **2019**, *15*, 1804927. [CrossRef]
21. Shivran, N.; Tyagi, M.; Mula, S.; Gupta, P.; Saha, B.; Patro, B.S.; Chattopadhyay, S. Syntheses and photodynamic activity of some glucose-conjugated BODIPY dyes. *Eur. J. Med. Chem.* **2016**, *122*, 352–365. [CrossRef] [PubMed]
22. Ramu, V.; Gautam, S.; Garai, A.; Kondaiah, P.; Chakravarty, A.R. Glucose-appended platinum(II)-BODIPY conjugates for targeted photodynamic therapy in red light. *Inorg. Chem.* **2018**, *57*, 1717–1726. [CrossRef] [PubMed]

23. Dai, X.; Chen, X.; Zhao, Y.; Yu, Y.; Wei, X.; Zhang, X.; Li, C. A water-soluble galactose-decorated cationic photodynamic therapy agent based on BODIPY to selectively eliminate biofilm. *Biomacromolecules* **2018**, *19*, 141–149. [CrossRef]
24. Treekoon, J.; Pewklang, T.; Chansaenpak, K.; Gorantla, J.N.; Pengthaisong, S.; Lai, R.-Y.; Ketudat-Cairns, J.R.; Kamkaew, A. Glucose conjugated aza-BODIPY for enhanced photodynamic cancer therapy. *Org. Biomol. Chem.* **2021**, *19*, 5867–5875. [CrossRef] [PubMed]
25. Gündüz, E.Ö.; Gedik, E.M.; Günaydin, G.; Okutan, E. Amphiphilic fullerene-BODIPY photosensitizers for targeted photodynamic therapy. *ChemMedChem* **2021**, e202100693. [CrossRef] [PubMed]
26. Feng, W.; Lv, Y.; Chen, Z.; Wang, F.; Wang, Y.; Pei, Y.; Jin, W.; Shi, C.; Wang, Y.; Qu, Y.; et al. A carrier-free multifunctional nano photosensitizer based on self-assembly of lactose-conjugated BODIPY for enhanced anti-tumor efficacy of dual phototherapy. *Chem. Eng. J.* **2021**, *417*, 129178. [CrossRef]
27. Yu, C.; Gao, Y.; Zhang, Y.; Wang, J.; Zhang, Y.; Li, J.; Zhang, X.; Wu, Z.; Zhang, X. A targeted photosensitizer mediated by visible light for efficient therapy of bacterial keratitis. *Biomacromolecules* **2021**, *22*, 3704–3717. [CrossRef] [PubMed]
28. Gomez, A.M.; Lopez, J.C. Bringing color to sugars: The chemical assembly of carbohydrates to BODIPY dyes. *Chem. Rec.* **2021**, *21*, 3112–3130. [CrossRef]
29. Liu, J.-Y.; Yeung, H.-S.; Xu, W.; Li, X.; Ng, D.K.P. Highly efficient energy transfer in subphthalocyanine-BODIPY conjugates. *Org. Lett.* **2008**, *10*, 5421–5424. [CrossRef]
30. Eaton, D.F. Reference materials for fluorescence measurement. *Pure Appl. Chem.* **1988**, *60*, 1107–1114. [CrossRef]
31. Scalise, I.; Durantini, E.N. Synthesis, properties, and photodynamic inactivation of Escherichia coli using a cationic and a noncharged Zn(II) pyridyloxyphthalocyanine derivatives. *Bioorg. Med. Chem.* **2005**, *13*, 3037–3045. [CrossRef] [PubMed]
32. Maree, M.D.; Kuznetsova, N.; Nyokong, T. Silicon octaphenoxyphthalocyanines: Photostability and singlet oxygen quantum yields. *J. Photochem. Photobiol. A Chem.* **2001**, *140*, 117–125. [CrossRef]
33. Tada, H.; Shiho, O.; Kuroshima, K.-I.; Koyama, M.; Tsukamoto, K. An improved colorimetric assay for interleukin 2. *J. Immunol. Methods* **1986**, *93*, 157–165. [CrossRef]
34. Zou, J.; Yin, Z.; Ding, K.; Tang, Q.; Li, J.; Si, W.; Shao, J.; Zhang, Q.; Huang, W.; Dong, X. BODIPY derivatives for photodynamic therapy: Influence of configuration versus heavy atom effect. *ACS Appl. Mater. Interfaces* **2017**, *9*, 32475–32481. [CrossRef] [PubMed]
35. Quagliotto, P.; Viscardi, G.; Barolo, C.; D'Angelo, D.; Barni, E.; Compari, C.; Duce, E.; Fisicaro, E. Synthesis and properties of new glucocationic surfactants: Model structures for marking cationic surfactants with carbohydrates. *J. Org. Chem.* **2005**, *70*, 9857–9866. [CrossRef]
36. He, H.; Lo, P.-C.; Yeung, S.-L.; Fong, W.-P.; Ng, D.K.P. Synthesis and in vitro photodynamic activities of pegylated boron dipyrromethene derivatives. *J. Med. Chem.* **2011**, *54*, 3097–3102. [CrossRef]
37. Zhou, Y.; Cheung, Y.-K.; Ma, C.; Zhao, S.; Gao, D.; Lo, P.-C.; Fong, W.-P.; Wong, K.S.; Ng, D.K.P. Endoplasmic reticulum-localized two-photon-absorbing boron dipyrromethenes as advanced photosensitizers for photodynamic therapy. *J. Med. Chem.* **2018**, *61*, 3952–3961. [CrossRef]
38. Szablewski, L. Expression of glucose transporters in cancers. *Biochim. Biophys. Acta* **2013**, *1835*, 164–169. [CrossRef]
39. Scafoglio, C.R.; Villegas, B.; Abdelhady, G.; Bailey, S.T.; Liu, J.; Shirali, A.S.; Wallace, W.D.; Magyar, C.E.; Grogan, T.R.; Elashoff, D.; et al. Sodium-glucose transporter 2 is a diagnostic and therapeutic target for early-stage lung adenocarcinoma. *Sci. Transl. Med.* **2018**, *10*, eaat5933. [CrossRef]
40. Zhou, J.; Zhu, J.; Yu, S.-J.; Ma, H.-L.; Chen, J.; Ding, X.-F.; Chen, G.; Liang, Y.; Zhang, Q. Sodium-glucose co-transporter-2 (SGLT-2) inhibition reduces glucose uptake to induce breast cancer cell growth arrest through AMPK/mTOR pathway. *Biomed. Pharmacother.* **2020**, *132*, 110821. [CrossRef]
41. Gruenberg, J. The endocytic pathway: A mosaic of domains. *Nat. Rev. Mol. Cell Biol.* **2001**, *2*, 721–730. [CrossRef] [PubMed]